A thin-film extensional flow model for biofilm expansion by sliding motility — electronic supplementary material

Alexander Tam*[1], J. Edward F. Green[1], Sanjeeva Balasuriya[1], Ee Lin Tek[2], Jennifer M. Gardner[2], Joanna F. Sundstrom[2], Vladimir Jiranek[2], and Benjamin J. Binder[1]

[1]School of Mathematical Sciences, University of Adelaide, Adelaide, SA 5005, Australia.
[2]Department of Wine and Food Science, Waite Campus, University of Adelaide, Urrbrae, SA 5064, Australia.

July 3, 2019

1 Parameter estimation

To obtain appropriate values for the parameters listed in Table 1, we require estimates for all dimensional quantities in (3.1), (3.3) and (3.5). In lieu of an accurate experimental measurement, we will assume that the thin-film parameter $\varepsilon = 0.1$. This is the same value used in the extensional flow model of Ward and King [1], and signifies that the biofilm thickness is an order of magnitude smaller than its radius. Accordingly, we also assume the initial biofilm height is $H_0 = 0.1$.

The experimental design also enables us to estimate several parameters. For example, the mean initial biofilm radius across the thirteen experiments in Tam et al. [2] was $R_b = 2.875\,\text{mm}$. The radius of the medium on which the biofilms were grown was 41.5 mm [3], giving $R = 14.4$. We use the physical properties of glucose to estimate parameters related to the nutrients. Using the same method as Tam et al. [2], we estimate the diffusion coefficient of glucose in agar to be $D_s = 4.01 \times 10^{-2}\,\text{mm}^2 \cdot \text{min}^{-1}$ [4, 5]. For the mass transfer coefficient of nutrients within the biofilm, we cite Vicente et al. [6], who estimate the mass transfer coefficient of glucose in a yeast (*S. cerevisiae*) floc to be $Q = 2.92 \times 10^{-3}\,\text{mm} \cdot \text{min}^{-1}$. Stewart [7] conducted a review of experimental measurements of diffusivity in biofilms of different bacterial and fungal species. They found that the average effective diffusivity of glucose in a microbial biofilm was $0.24D_{aq}$, where $D_{aq} = 4.04 \times 10^{-2}\,\text{mm}^2 \cdot \text{min}^{-1}$ is the diffusivity of glucose in water [5]. Thus, a suitable estimate is $D_b = 9.70 \times 10^{-3}\,\text{mm}^2 \cdot \text{min}^{-1}$. This is of the same order of magnitude as an estimate for colony of *S. cerevisiae*, which Vicente et al. [6] give as $D_b = 6.6 \times 10^{-3}\,\text{mm}^2 \cdot \text{min}^{-1}$.

The cell production rate ψ_n and nutrient consumption rate η are chosen to minimise the sum of squared differences between numerical solutions and the experimental data.

*Corresponding author: alexander.tam@adelaide.edu.au

We found that the combination of $\psi_n = 12.1\,\mathrm{mm}^2 \cdot \mathrm{g}^{-1} \cdot \mathrm{min}^{-1}$ and $\eta = 3.7 \times 10^{-3}\,\mathrm{min}^{-1}$ produced a local minimum in the error, and therefore we adopted these as our parameter estimates. At the same time, we estimate the ECM production rate ψ_m using the experimental observation that extracellular material occupies approximately 10% of mature *S. cerevisiae* mats by volume, and therefore assume $\Psi_m = 1/9$. This is now sufficient to determine representative values for all of the dimensionless parameters in Table 1.

2 Numerical method

As mentioned in §4 (a), before solving the 1D radial model numerically, we apply the change of variables (4.1) to map both the biofilm and unoccupied Petri dish domains to the unit interval. The governing equations to solve then become

$$\frac{\partial h}{\partial t} - \frac{\xi}{S}\frac{\mathrm{d}S}{\mathrm{d}t}\frac{\partial h}{\partial \xi} + \frac{1}{S\xi}\frac{\partial}{\partial \xi}\left(\xi u_r h\right) = \left(1+\Psi_m\right)\bar{\phi}_n g_b h, \tag{ESM–2.1a}$$

$$\frac{\partial \bar{\phi}_n}{\partial t} + \frac{1}{S}\left(u_r - \xi\frac{\mathrm{d}S}{\mathrm{d}t}\right)\frac{\partial \bar{\phi}_n}{\partial \xi} = \bar{\phi}_n\left[g_b - \Psi_d - \left(1+\Psi_m\right)\bar{\phi}_n g_b\right], \tag{ESM–2.1b}$$

$$\frac{\partial g_s}{\partial t} - \frac{\xi}{S}\frac{\mathrm{d}S}{\mathrm{d}t}\frac{\partial g_s}{\partial \xi} = \frac{D}{S^2\xi}\frac{\partial}{\partial \xi}\left(\xi\frac{\partial g_s}{\partial \xi}\right) - DQ_s\left(g_s - g_b\right), \tag{ESM–2.1c}$$

$$\begin{aligned}\frac{\partial g_{s_o}}{\partial t} + \frac{1-\xi_o}{R-S}\frac{\mathrm{d}S}{\mathrm{d}t}\frac{\partial g_{s_o}}{\partial \xi_o} &= \frac{D}{(R-S)^2}\frac{\partial^2 g_{s_o}}{\partial \xi_o^2} \\ &+ \frac{D}{S(R-S)+\xi_o(R-S)^2}\frac{\partial g_{s_o}}{\partial \xi_o},\end{aligned} \tag{ESM–2.1d}$$

$$\begin{aligned}\mathrm{Pe}\left\{h\frac{\partial g_b}{\partial t} - h\frac{\xi}{S}\frac{\mathrm{d}S}{\mathrm{d}t}\frac{\partial g_b}{\partial \xi} + \frac{1}{S\xi}\frac{\partial}{\partial \xi}\left[\xi u_r\left(1-\bar{\phi}_n\right)g_b h\right]\right\} = \\ \frac{1}{S^2\xi}\frac{\partial}{\partial \xi}\left(\xi h\frac{\partial g_b}{\partial \xi}\right) + Q_b\left(g_s - g_b\right) - \Upsilon\bar{\phi}_n g_b h,\end{aligned} \tag{ESM–2.1e}$$

$$\begin{aligned}\frac{4}{S}\frac{\partial}{\partial \xi}\left[\frac{h}{\xi}\frac{\partial}{\partial \xi}\left(\xi u_r\right)\right] - \frac{2u_r}{S\xi}\frac{\partial h}{\partial \xi} = 2\left(1+\Psi_m\right)\frac{\partial}{\partial \xi}\left(\bar{\phi}_n g_b h\right) \\ -\frac{\gamma^* h}{S^2}\frac{\partial}{\partial \xi}\left[\frac{1}{\xi}\frac{\partial}{\partial \xi}\left(\xi\frac{\partial h}{\partial \xi}\right)\right],\end{aligned} \tag{ESM–2.1f}$$

$$\frac{\mathrm{d}S}{\mathrm{d}t} = u_r\left(1,t\right), \tag{ESM–2.1g}$$

where g_{s_o} denotes the nutrient concentration in the region of the substratum that is not occupied by the biofilm. Under the change of variables (4.1), the initial conditions are

$$\begin{gathered} S(0)=1, \quad h(\xi,0)=H_0\left(1-\xi^2\right), \quad \bar{\phi}_n(\xi,0)=1, \\ g_s(\xi,0)=g_{s_o}(\xi_o,0)=1, \quad g_b(\xi,0)=0, \end{gathered} \tag{ESM–2.2}$$

the boundary conditions become

$$\begin{gathered} \left.\frac{\partial h}{\partial \xi}\right|_{(0,t)}=0, \quad \left.\frac{\partial \bar{\phi}_n}{\partial \xi}\right|_{(0,t)}=0, \quad \left.\frac{\partial g_s}{\partial \xi}\right|_{(0,t)}=0, \quad \left.\frac{\partial g_b}{\partial \xi}\right|_{(0,t)}=0, \quad u_r(0,t)=0, \\ \left.\frac{\partial g_{s_o}}{\partial \xi_o}\right|_{(1,t)}=0, \quad \left.\frac{\partial g_b}{\partial \xi}\right|_{(1,t)}=0, \\ \left.\frac{4}{S}\frac{\partial u_r}{\partial \xi}\right|_{(1,t)}+\frac{2u_r(1,t)}{S}=2\left(1+\Psi_m\right)\bar{\phi}_n(1,t)g_b(1,t)-\frac{\gamma^*}{S^2}\left.\frac{\partial}{\partial \xi}\left(\xi\frac{\partial h}{\partial \xi}\right)\right|_{(1,t)}, \end{gathered} \tag{ESM–2.3}$$

and we must also satisfy the continuity conditions

$$g_s\left(1,t\right)=g_{s_o}\left(0,t\right), \quad \left.\frac{1}{S}\frac{\partial g_s}{\partial \xi}\right|_{(1,t)}=\frac{1}{R-S}\left.\frac{\partial g_{s_o}}{\partial \xi_o}\right|_{(0,t)}. \tag{ESM–2.4}$$

Producing a numerical solution to the 1D axisymmetric extensional flow model then requires solving the system (ESM–2.1), subject to (ESM–2.2)–(ESM–2.4), on $\xi \in [0,1]$, $\xi_o \in [0,1]$, and $t \in [0,T]$.

We solve the model on equispaced grids in time and space. For the time domain, we denote the discrete grid points by $t^k=(k-1)\Delta t$, for $k=1,\ldots,N_t$, where $\Delta t = T/(N_t-1)$. For both the biofilm and outer Petri dish domains, we define $\xi_j=(j-1)\Delta\xi$ and $\xi_{oj}=(j-1)\Delta\xi_o$ for $j=1,\ldots,N_\xi$, where $\Delta\xi=1/(N_\xi-1)$ and $\Delta\xi_o=1/(N_{\xi_o}-1)$, to represent the discrete grid points. After prescribing the initial conditions, we first solve (ESM–2.1f) to determine the initial fluid velocity. Following this, at each time step we solve the equations in the order listed in (ESM–2.1), until the final time $t^{N_t}=T$ is reached.

We discretise the governing equations using a finite difference Crank–Nicolson scheme. Where necessary, we linearise nonlinear terms using data from the previous time step. In the equations for h and u_r, we first expand relevant derivative terms using the product rule before discretising the equations. At the interior grid points $j=2,\ldots N_\xi-1$, the numerical scheme then reads

$$\begin{aligned} &\frac{h_j^k-h_j^{k-1}}{\Delta t}+\left(\frac{{u_r}_j^{k-1}-\xi_j{u_r}_{N_\xi}^{k-1}}{S^{k-1}}\right)\frac{h_{j+1}^{k-1/2}-h_{j-1}^{k-1/2}}{2\Delta\xi} \\ &+\left(\frac{{u_r}_{j+1}^{k-1}-{u_r}_{j-1}^{k-1}}{2S^{k-1}\Delta\xi}+\frac{{u_r}_j^{k-1}}{S^{k-1}\xi_j}\right)h_j^{k-1/2}=\left(1+\Psi_m\right)\bar{\phi}_{n_j}^{k-1}{g_b}_j^{k-1}h_j^{k-1/2}, \end{aligned} \tag{ESM–2.5a}$$

$$\frac{\bar{\phi}_{n_j}^{\,k}-\bar{\phi}_{n_j}^{\,k-1}}{\Delta t}+\left(\frac{u_{r_j}^{\,k-1}-\xi_j u_{r_{N_\xi}}^{\,k-1}}{S^{k-1}}\right)\frac{\bar{\phi}_{n_{j+1}}^{\,k-1/2}-\bar{\phi}_{n_{j-1}}^{\,k-1/2}}{2\Delta\xi}$$
$$=\bar{\phi}_{n_j}^{\,k-1/2}\left[g_{b_j}^{k-1}-\Psi_d-(1+\Psi_m)\,\bar{\phi}_{n_j}^{\,k-1}g_{b_j}^{k-1}\right], \tag{ESM–2.5b}$$

$$\frac{g_{s_j}^{\,k}-g_{s_j}^{\,k-1}}{\Delta t}-\left(\frac{\xi_j u_{r_{N_\xi}}^{\,k-1}}{S^{k-1}}\right)\frac{g_{s_{j+1}}^{\,k-1/2}-g_{s_{j-1}}^{\,k-1/2}}{2\Delta\xi}$$
$$=\frac{D}{\left(S^{k-1}\right)^2\xi_j}\left[\frac{(\xi_{j+1}+\xi_j)\left(g_{s_{j+1}}^{\,k-1/2}-g_{s_j}^{\,k-1/2}\right)}{2\left(\Delta\xi\right)^2}\right]$$
$$-\frac{D}{\left(S^{k-1}\right)^2\xi_j}\left[\frac{(\xi_j+\xi_{j-1})\left(g_{s_j}^{\,k-1/2}-g_{s_{j-1}}^{\,k-1/2}\right)}{2\left(\Delta\xi\right)^2}\right] \tag{ESM–2.5c}$$
$$-DQ_s\left(g_{s_j}^{\,k-1/2}-g_{b_j}^{k-1}\right),$$

$$\frac{g_{s_{oj}}^{\,k}-g_{s_{oj}}^{\,k-1}}{\Delta t}+\left(\frac{1-\xi_{oj}}{R-S^{k-1}}u_{r_{N_\xi}}^{\,k-1}\right)\frac{g_{s_{oj+1}}^{\,k-1/2}-g_{s_{oj-1}}^{\,k-1/2}}{2\Delta\xi_o}$$
$$=\frac{D}{\left(R-S^{k-1}\right)^2}\frac{g_{s_{oj+1}}^{\,k-1/2}-2g_{s_{oj}}^{\,k-1/2}+g_{s_{oj-1}}^{\,k-1/2}}{\left(\Delta\xi_o\right)^2} \tag{ESM–2.5d}$$
$$+\left[\frac{D}{S^{k-1}\left(R-S^{k-1}\right)+\xi_{oj}\left(R-S^{k-1}\right)^2}\right]\frac{g_{s_{oj+1}}^{\,k-1/2}-g_{s_{oj-1}}^{\,k-1/2}}{2\Delta\xi},$$

$$\mathrm{Pe}h_j^{k-1}\frac{g_{b_j}^{\,k}-g_{b_j}^{\,k-1}}{\Delta t}-\left(\frac{\mathrm{Pe}h_j^{k-1}\xi_j u_{r_{N_\xi}}^{\,k-1}}{S^{k-1}}\right)\frac{g_{b_{j+1}}^{\,k-1/2}-g_{b_{j-1}}^{\,k-1/2}}{2\Delta\xi}$$
$$+\frac{\mathrm{Pe}}{S^{k-1}\xi_j}\frac{\left[\xi u_r\left(1-\bar{\phi}_n\right)h\right]_{j+1}^{k-1}g_{b_{j+1}}^{\,k-1/2}-\left[\xi u_r\left(1-\bar{\phi}_n\right)h\right]_{j-1}^{k-1}g_{b_{j-1}}^{\,k-1/2}}{2\Delta\xi}$$
$$=\frac{1}{\left(S^{k-1}\right)^2\xi_j}\left[\frac{\left(\xi_{j+1}h_{j+1}^{k-1}+\xi_j h_j^{k-1}\right)\left(g_{b_{j+1}}^{\,k-1/2}-g_{b_j}^{\,k-1/2}\right)}{2\left(\Delta\xi\right)^2}\right] \tag{ESM–2.5e}$$
$$-\frac{1}{\left(S^{k-1}\right)^2\xi_j}\left[\frac{\left(\xi_j h_j^{k-1}+\xi_{j-1}h_{j-1}^{k-1}\right)\left(g_{b_j}^{\,k-1/2}-g_{b_{j-1}}^{\,k-1/2}\right)}{2\left(\Delta\xi\right)^2}\right]$$
$$+Q_b\left(g_{s_j}^{\,k-1}-g_{b_j}^{\,k-1/2}\right)-\Upsilon\bar{\phi}_{n_j}^{\,k-1}g_{b_j}^{\,k-1/2}h_j^{k-1},$$

$$\left(\frac{4h_j^k}{S^{k-1}}\right)\frac{u_{rj+1}^k - 2u_{rj}^k + u_{rj-1}^k}{(\Delta\xi)^2} + \frac{4}{S^{k-1}}\left(\frac{h_{j+1}^k - h_{j-1}^k}{2\Delta\xi} + \frac{h_j^k}{\xi_j}\right)\frac{u_{rj+1}^k - u_{rj-1}^k}{2\Delta\xi} + \frac{2}{S^{k-1}\xi_j}\left(\frac{h_{j+1}^k - h_{j-1}^k}{2\Delta\xi} - \frac{2h_j^k}{\xi_j}\right)u_{rj}^k = 2\left(1+\Psi_m\right)\left[\frac{\left(\bar{\phi}_n g_b h\right)_{j+1}^k - \left(\bar{\phi}_n g_b h\right)_{j-1}^k}{2\Delta\xi}\right] - \Gamma_j^k, \tag{ESM–2.5f}$$

$$\frac{S^k - S^{k-1}}{\Delta t} = u_{rN_\xi}^{k-1/2}, \tag{ESM–2.5g}$$

where we approximate terms at the half time points using

$$h_j^{k-1/2} = \frac{h_j^k + h_j^{k-1}}{2}, \tag{ESM–2.6}$$

and so on. In (ESM–2.5f), Γ_j^k denotes the discretised surface tension term, which we discuss in detail later. In conjunction with appropriate boundary schemes, each equation in (ESM–2.5) describes a linear system to solve for the variables at $t = t^k$.

We need to take particular care at domain boundaries to prevent spurious oscillations appearing in the solution. At $\xi = 0$ and $\xi_o = 0$, we obtained the best results by substituting the boundary conditions into discretised forms of the equations (ESM–2.1c) and (ESM–2.1e), using one-sided differences for first derivative terms and introducing fictitious grid points for second derivative terms. For (ESM–2.1a), (ESM–2.1b), (ESM–2.1d) and (ESM–2.1f) we apply the relevant boundary conditions explicitly. Although the equations (ESM–2.1c) and (ESM–2.1e) are singular at $\xi = 0$, we can use L'Hôpital's rule to evaluate the relevant terms as $\xi \to 0$. The boundary schemes are then

$$\frac{-3h_1^k + 4h_2^k - h_3^k}{2\Delta\xi} = 0, \tag{ESM–2.7a}$$

$$\frac{-3\phi_{n1}^k + 4\phi_{n2}^k - \phi_{n3}^k}{2\Delta\xi} = 0, \tag{ESM–2.7b}$$

$$\frac{g_{s1}^k - g_{s1}^{k-1}}{\Delta t} = \frac{4D}{(S^{k-1})^2}\frac{g_{s2}^{k-1/2} - g_{s1}^{k-1/2}}{(\Delta\xi)^2} - DQ_s\left(g_{s1}^{k-1/2} - g_{b1}^{k-1}\right), \tag{ESM–2.7c}$$

$$g_{so1}^k = a, \tag{ESM–2.7d}$$

$$\begin{aligned}
&\mathrm{Pe} h_1^{k-1} \frac{g_{b1}^k - g_{b1}^{k-1}}{\Delta t} \\
&+ \frac{\mathrm{Pe}\left(1-\bar{\phi}_{n1}^{k-1}\right) h_1^{k-1}\left(-3u_{r1}^{k-1}+4u_{r2}^{k-1}-u_{r3}^{k-1}\right)}{S^{k-1}\Delta\xi} g_{b1}^{k-1/2} \\
&= \frac{4h_1^{k-1}}{\left(S^{k-1}\right)^2}\frac{g_{b2}^{k-1/2}-g_{b1}^{k-1/2}}{(\Delta\xi)^2} + Q_b\left(g_{b1}^{k-1/2}-g_{s1}^k\right) \\
&\quad -\Upsilon\bar{\phi}_{n1}^{k-1} g_{b1}^{k-1/2} h_1^{k-1},
\end{aligned} \tag{ESM–2.7e}$$

$$u_{r1}^k = 0, \tag{ESM–2.7f}$$

where a is the value of $g_s(S(t),t)$. At $\xi = 1$ and $\xi_o = 1$, we solve the equations (ESM–2.1a), (ESM–2.1b) and (ESM–2.1d) directly, again using one-sided differences for first derivatives and introducing fictitious grid points for second derivatives. We apply the Dirichlet condition for g_s, and as (ESM–2.1e) is singular as $h \to 0$, we impose the boundary condition for g_b directly using a one-sided difference. We also obtained best results by applying the zero radial stress condition directly at $\xi = 1$. The boundary schemes are then

$$\begin{aligned}
&\frac{h_{N_\xi}^k - h_{N_\xi}^{k-1}}{\Delta t} + \left(\frac{3u_{rN_\xi}^{k-1} - 4u_{rN_\xi-1}^{k-1} + u_{rN_\xi-2}^{k-1}}{2S^{k-1}\Delta\xi} + \frac{u_{rN_\xi}^{k-1}}{S^{k-1}}\right) h_{N_\xi}^{k-1/2} \\
&\qquad = (1+\Psi_m)\,\bar{\phi}_{nN_\xi}^{k-1} g_{bN_\xi}^{k-1} h_{N_\xi}^{k-1/2},
\end{aligned} \tag{ESM–2.8a}$$

$$\frac{\bar{\phi}_{nN_\xi}^k - \bar{\phi}_{nN_\xi}^{k-1}}{\Delta t} = \bar{\phi}_{nN_\xi}^{k-1/2}\left[g_{bN_\xi}^{k-1} - \Psi_d - (1+\Psi_m)\,\bar{\phi}_{nN_\xi}^{k-1} g_{bN_\xi}^{k-1}\right], \tag{ESM–2.8b}$$

$$g_{sN_\xi}^k = a, \tag{ESM–2.8c}$$

$$\frac{g_{soN_\xi}^k - g_{soN_\xi}^{k-1}}{\Delta t} = \frac{D}{(R-S)^2}\frac{2g_{soN_\xi-1}^{k-1/2} - 2g_{soN_\xi}^{k-1/2}}{(\Delta\xi)^2}, \tag{ESM–2.8d}$$

$$\frac{3g_{bN_\xi}^k - 4g_{bN_\xi-1}^k + g_{bN_\xi-2}^k}{2\Delta\xi} = 0, \tag{ESM–2.8e}$$

$$\begin{aligned}
&\frac{2}{S^{k-1}}\left(\frac{3u_{rN_\xi}^k - 4u_{rN_\xi-1}^k + u_{rN_\xi-2}^k}{\Delta\xi} + u_{rN_\xi}^k\right) \\
&\qquad = 2\,(1+\Psi_m)\,\bar{\phi}_{nN_\xi}^k g_{bN_\xi}^k - \Gamma_{N_\xi}^k,
\end{aligned} \tag{ESM–2.8f}$$

where $\Gamma_{N_\xi}^k$ is the contribution of surface tension to the no radial stress boundary condition in (ESM–2.3).

For the surface tension terms, we expand the derivative terms and write

$$\Gamma_j^k = \frac{h_j^k}{\left(S^k\right)^2}\left[\frac{\partial^3 h}{\partial\xi^3} + \frac{1}{\xi}\frac{\partial^2 h}{\partial\xi^2} - \frac{1}{\xi^2}\frac{\partial h}{\partial\xi}\right]_j^k, \qquad \text{for} \quad j = 2,\ldots N_\xi - 1, \tag{ESM–2.9a}$$

$$\Gamma^k_{N_\xi} = \frac{1}{(S^k)^2}\left[\xi\frac{\partial^2 h}{\partial \xi^2} + \frac{\partial h}{\partial \xi}\right]^k_{N_\xi}. \tag{ESM–2.9b}$$

To compute the first spatial derivative of h, we use standard sixth-order accurate finite difference formulae. We then use the same scheme to compute the higher derivatives sequentially, that is

$$\frac{\partial^2 h}{\partial \xi^2} = \frac{\partial}{\partial \xi}\left(\frac{\partial h}{\partial \xi}\right), \quad \text{and} \quad \frac{\partial^3 h}{\partial \xi^3} = \frac{\partial}{\partial \xi}\left[\frac{\partial}{\partial \xi}\left(\frac{\partial h}{\partial \xi}\right)\right], \tag{ESM–2.10}$$

where we represent differentiation operators with the finite difference scheme. When $\gamma^* \neq 0$, we required a larger number of time steps to produce solutions without spurious oscillations in the surface tension term. Therefore, all solutions involving surface tension were computed with $N_\xi = 1001$ and $N_t = 2000001$. The convergence analysis in §2.1 suggests that this will produce solutions that are accurate to approximately 0.4% relative error.

A feature of our model is that finding the nutrient concentration in the substratum requires solving both (ESM–2.1c) and (ESM–2.1d), and ensuring that the continuity conditions (ESM–2.4) are satisfied. To do this, we first solve (ESM–2.1c) and (ESM–2.1d), in both cases assuming the Dirichlet conditions $g_s(1,t^k) = g_{s_o}(0,t^k) = a$, with $a = g_s(1,t^{k-1})$, as an initial guess. To ensure continuity of the derivative, we define and compute

$$f(a) = \frac{1}{R-S}\frac{\partial g_{s_o}}{\partial \xi_o}\bigg|_{(0,t)} - \frac{1}{S}\frac{\partial g_s}{\partial \xi}\bigg|_{(1,t)}, \tag{ESM–2.11}$$

for the initial guess of a, with both derivatives in (ESM–2.11) approximated using second-order one-sided finite differences. We then use Newton's method to drive $f(a)$ to zero, where we approximate the required derivative numerically using

$$\frac{\mathrm{d}f}{\mathrm{d}a} = \frac{f(a+\delta) - f(a)}{\delta}, \tag{ESM–2.12}$$

for $\delta = 1 \times 10^{-6}$, and iterate until a is accurate to 1×10^{-6}. This procedure allows us to solve for g_s over the entire Petri dish domain at each time step.

2.1 Convergence of the numerical method

The numerical solutions in §4 (a) were computed using $N_\xi = 8001$ grid points and $N_t = 160001$ time steps, giving $\Delta\xi = 1.25 \times 10^{-4}$ and $\Delta t \approx 1 \times 10^{-4}$. To verify that this is sufficient to produce a converged solution, we repeated the computation using a range of grid spacings and time step sizes. In each case, we computed the contact line position at $t = 15.9$, which yielded the results shown in Figure 2.1. The numerical scheme

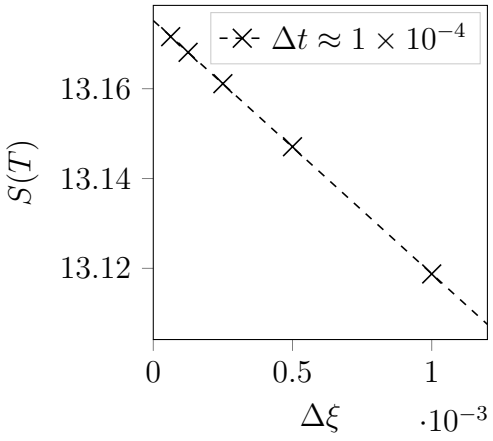

(a) Numerical results for $\Delta t \approx 1 \times 10^{-4}$, and $\Delta\xi \to 0$.

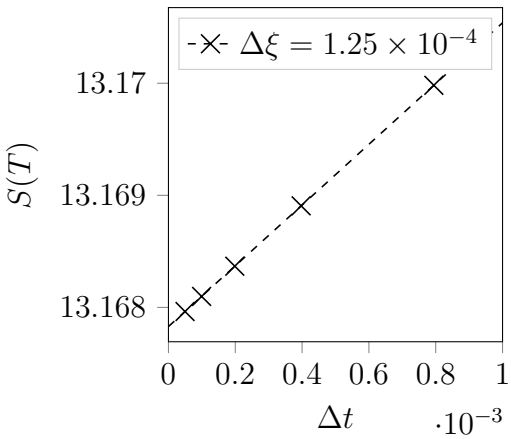

(b) Numerical results for $\Delta\xi = 1.25 \times 10^{-4}$, and $\Delta t \to 0$.

Figure 2.1: Convergence of the numerical scheme for the axisymmetric extensional flow model. At each data point, we plot the biofilm radius attained at the experimental time $t = T$.

exhibits linear convergence with both grid spacing and time step size. By fitting a straight line to the data in Figure 2.1 and extrapolating, we can estimate the numerical contact line position in the zero grid spacing and time step limit. Doing so, we find that when $\Delta t \approx 1 \times 10^{-4}$, the estimated contact line position as $\Delta\xi \to 0$ is $S(T) = 13.1752$. When $\Delta\xi = 1.25 \times 10^{-4}$, the estimated contact line position as $\Delta t \to 0$ is $S(T) = 13.1678$. As these are within approximately 0.05% of each other and the numerical value for the chosen grid spacing and time step size, $S(T) = 13.1681$, we conclude that our numerical solution is sufficiently converged.

3 Statements

3.1 Ethics

No ethical approval was required for this research.

3.2 Data, code, and materials

Data and code for this research are available at The University of Adelaide's Figshare repository, at https://doi.org/10.25909/5c93294133642, under a Creative Commons CC BY 4.0 license.

3.3 Competing interests

The authors declare no competing interests.

3.4 Author contributions

All authors designed the research. A. T. performed the mathematical modelling and numerical computation, with assistance from B. J. B., J. E. F. G., and S. B., and wrote the manuscript. E. L. T., J. M. G., and J. F. S. performed the mat formation experiments under supervision of V. J., and collected the data. All authors provided comments and guidance on the manuscript.

References

[1] J. P. Ward and J. R. King, "Thin-film modelling of biofilm growth and quorum sensing", *J. Eng. Math.* 73 (2012), pp. 71–92, DOI: 10.1007/s10665-011-9490-4.

[2] A. Tam, J. E. F. Green, S. Balasuriya, E. L. Tek, J. M. Gardner, J. F. Sundstrom, V. Jiranek, and B. J. Binder, "Nutrient-limited growth with non-linear cell diffusion as a mechanism for floral pattern formation in yeast biofilms", *J. Theor. Biol.* 448 (2018), pp. 122–141, DOI: 10.1016/j.jtbi.2018.04.004.

[3] H. Tronnolone, A. Tam, Z. Szenczi, J. E. F. Green, S. Balasuriya, E. L. Tek, J. M. Gardner, J. F. Sundstrom, V. Jiranek, S. G. Oliver, and B. J. Binder, "Diffusion-limited growth of microbial colonies", *Sci. Rep.* 8 (2018), pp. 1–11, DOI: 10.1038/s41598-018-23649-z.

[4] A. L. Slade, A. E. Cremers, and H. C. Thomas, "The obstruction effect in the self-diffusion coefficients of sodium and cesium in agar gels", *J. Phys. Chem.* 70 (1966), pp. 2840–2844, DOI: 10.1021/j100881a020.

[5] L. G. Longsworth, "Electrochemistry in biology and medicine", ed. by T. Shedlovsky, John Wiley & Sons, Inc., 1955, chap. 12: Diffusion in liquids and the Stokes–Einstein relation, pp. 225–247, DOI: 10.1016/0002-8703(55)90290-8.

[6] A. A. Vicente, M. Dluhý, E. C. Ferreira, M. Mota, and J. A. Teixeira, "Mass transfer properties of glucose and O_2 in *Saccharomyces cerevisiae* flocs", *Biochem. Eng. J.* 2 (1998), pp. 35–43, DOI: 10.1016/S1369-703X(98)00015-1.

[7] P. S. Stewart, "A review of experimental measurements of effective diffusive permeabilities and effective diffusion coefficients in biofilms", *Biotechnol. Bioeng.* 59 (1998), pp. 261–272, DOI: 10.1002/(SICI)1097-0290(19980805)59:3<261::AID-BIT1>3.0.CO;2-9.